Cell, Vol. 115, 739–750, December 12, 2003, Copyright ©2003 by Cell Press

Ribosome Loading onto the mRNA Cap Is Driven by Conformational Coupling between eIF4G and eIF4E

John D. Gross,[1,5] Nathan J. Moerke,[1,2] Tobias von der Haar,[3] Alexey A. Lugovskoy,[1] Alan B. Sachs,[4] John E.G. McCarthy,[3] and Gerhard Wagner[1,*]

[1]Department of Biological Chemistry and Molecular Pharmacology
[2]Graduate Program in Biological and Biomedical Science
Harvard Medical School
Boston, Massachusetts 02115
[3]Posttranscriptional Control Group
Department of Biomolecular Sciences
University of Manchester Institute of Science and Technology
Manchester M60 1QD
United Kingdom
[4]Department of Molecular and Cell Biology
University of California at Berkeley
Berkeley, California 94720

Summary

The eukaryotic initiation factor 4G (eIF4G) is the core of a multicomponent switch controlling gene expression at the level of translation initiation. It interacts with the small ribosomal subunit interacting protein, eIF3, and the eIF4E/cap-mRNA complex in order to load the ribosome onto mRNA during cap-dependent translation. We describe the solution structure of the complex between yeast eIF4E/cap and eIF4G (393–490). Binding triggers a coupled folding transition of eIF4G (393–490) and the eIF4E N terminus resulting in a molecular bracelet whereby eIF4G (393–490) forms a right-handed helical ring that wraps around the N terminus of eIF4E. Cofolding allosterically enhances association of eIF4E with the cap and is required for maintenance of optimal growth and polysome distributions in vivo. Our data explain how mRNA, eIF4E, and eIF4G exists as a stable mRNP that may facilitate multiple rounds of ribosomal loading during translation initiation, a key determinant in the overall rate of protein synthesis.

Introduction

Control of gene expression at the level of translation initiation is critical for cellular proliferation, development, differentiation, and death. In eukaryotes, a panoply of initiation factors (eIFs) are required to dissociate the 40S and 60S ribosomal subunits, to recruit and ensure proper positioning of mRNA and initiator tRNA relative to the small ribosomal subunit, and to promote joining of the loaded small subunit together with the large subunit thereby enabling elongation (Dever, 2002; Hershey and Merrick, 2000). The localization of the 5′ end of the mRNA to the small ribosomal subunit is thought to be the major rate-controlling step in translation initiation. The process is subject to precise regulation and requires the step-wise assembly of a large multiprotein complex. At the center of this network is eIF4G (Dever, 2002; Hentze, 1997): a multidomain protein that interacts with eIF4E, eIF4A, the polyadenyl binding protein (PABP or Pab1p in yeast), and eIF3 (reviewed in Hershey and Merrick, 2000). eIF4E interacts with the m^7GpppX cap structure found on all nuclear-encoded messenger RNA while PABP engages the polyadenyl tail. In mammals, eIF3 binds the small ribosomal subunit (Benne and Hershey, 1976) and serves as an anchor for eIF4G (Lamphear et al., 1995) while in yeast, this function seems to be performed by eIFs 1, 3, and 5 in the context of a multifactor complex (Asano et al., 2001; He et al., 2003).

During cap-dependent translation, eIF4G brings the 5′ end of the mRNA in proximity with the helicase eIF4A through interactions with eIF4E. This configuration of factors (also termed eIF4F, reviewed in Gingras et al., 1999b) is thought to promote the migration of the small ribosomal subunit from the 5′ end of the mRNA in search of a start codon. The 4E binding proteins (4E-BPs) (Pause et al., 1994) block assembly of eIF4F through competition with eIF4G for a common surface on eIF4E (Haghighat et al., 1995). In *S. cerevisiae*, a related protein p20 (Altmann et al., 1997; Ptushkina et al., 1998) binds to this surface. Hyperphosphorylation of the 4E-BPs in response to growth factors and mitogens results in release of eIF4E, subsequent binding to eIF4G, and upregulation of cap-dependent translation (Raught et al., 2000). A consensus eIF4E binding motif consisting of $Y(X)_4L\phi$ (X variable, ϕ hydrophobic) is found on all 4E-BPs, p20, and eIF4G (Altmann et al., 1997; Mader et al., 1995). Structures of N terminally truncated murine eIF4E alone (Marcotrigiano et al., 1997), and in complex with sixteen residue peptides containing the $Y(X)_4L\phi$ region from mammalian 4E-BP1 and eIF4GII, have been reported (Marcotrigiano et al., 1999). These regions of 4E-BP and eIF4GII form a short helix and occupy a shared binding site on eIF4E. The conformation of eIF4E is unaltered when bound to either peptide.

Like the cap structure, the 3′ poly(A) tail is capable of influencing translation (Jacobson, 1996; Sachs et al., 1997). During early development, gene specific translational activation proceeds through cytoplasmic polyadenylation of nascent mRNA and subsequent assembly of the PABP/eIF4G/eIF4E complex (reviewed in Richter, 2000). The poly(A) tail is capable of supporting translation in the absence of the cap in vitro (Iizuka et al., 1994) and this effect depends on the interaction of eIF4G and PABP (Tarun and Sachs, 1997). Experiments performed both in vivo and in vitro have revealed that the cap and poly(A) tail can act synergistically to stimulate translation (Gallie, 1991; Iizuka et al., 1994). Synergy may arise from mRNA forming a closed loop around eIF4G through simultaneous interactions of the 5′ and 3′ termini via eIF4E and PABP or an alternative-bridging mechanism

*Correspondence: gerhard_wagner@hms.harvard.edu
[5]Present address: Department of Biochemistry and Molecular Pharmacology, University of Massachusetts Medical School, LRB 922, 364 Plantation Street, Worcester, Massachusetts 01604

(Uchida et al., 2002; Wells et al., 1998). A number of observations suggest that the termini of mRNA are able to communicate through allosteric interactions mediated by PABP, eIF4G, and eIF4E (reviewed in Prevot et al., 2003) and that these mutually reinforcing effects may promote translational synergy by generating a stable circular mRNP structure capable of supporting multiple initiation-termination-reinitiation cycles.

To better understand the structural basis for how signals are transmitted from eIF4G through eIF4E to the cap structure and how PABP might modulate such an effect, we have mapped the minimal eIF4E binding domain of yeast eIF4GI with a combination of genetic, biochemical, and biophysical methods (Hershey et al., 1999). Mutation of residues far removed from the $Y(X)_4L\phi$ region within a 98 residue region of full-length yeast eIF4GI abrogate binding to eIF4E. This region of yeast eIF4GI (residues 393–490) becomes structured upon binding eIF4E (Hershey et al., 1999). Here, we report the solution structure of eIF4GI (393–490) in complex with eIF4E. We show complex formation results in folding of the N terminus of eIF4E with concomitant folding of eIF4G through a mutually induced fit mechanism; protein binding alters the conformation and/or the stability of the cap binding slot resulting in enhanced association of eIF4E with the cap structure; dissociation of the ternary complex is slow; and the N terminus of eIF4E is required for these effects. Yeast strains harboring mutants of eIF4E lacking key N-terminal residues show impaired growth phenotypes, a decrease in polysome content and a reduced interaction between eIF4E and eIF4G in vivo. A structure-based model of how complex assembly is regulated by the 4E-BPs is then discussed.

Results and Discussion

Structure Determination of the eIF4E/m^{7}GDP/eIF4G Complex

The ternary complex between yeast eIF4E, eIF4G (393–490), and m^{7}GDP proved refractory to high-resolution crystallographic analysis (Hershey et al., 1999). We have solved the solution structure of yeast eIF4E in complex with m^{7}GDP and eIF4G (393–490), a 35 kDa complex containing 313 residues, using multidimensional NMR spectroscopy. As with the binary m^{7}GDP/eIF4E complex, the solubility of the ternary complex was increased by the presence of the nondenaturing detergent CHAPS (Matsuo et al., 1997).

A total of 275 intermolecular and 2685 intramolecular distance restraints were derived from NOE or paramagnetic broadening data and were used to generate an ensemble of 50 structures using the program XPLOR (Brunger, 1996). Stereo views of the best-fit superpositions (Figure 1C) and the statistical analysis for the structure calculations demonstrate that the calculations led to good convergence (Table 1). Except for the contact regions of eIF4E (labeled with filled circles in Figure 1A), chemical shifts of the eIF4E/m^{7}GDP portion of the complex were nearly identical to those of the binary eIF4E/m7GDP complex. Thus, constraints were adopted from the latter structure determination (Matsuo et al., 1997) for the unchanged portion of the ternary complex (see below and Experimental Procedures).

Structural Overview

Upon binding eIF4E, eIF4G (393–490) folds into an unusual closed ring-shaped structure consisting of five helical segments arranged from the N to C terminus in a right-handed fashion, culminating in a parallel alignment of the terminal helices (Figures 1C and 1D). The fourth helix (α_4) of eIF4G (393–490) contains the well-characterized eIF4E consensus binding motif including the $Y(X)_4L\phi$ sequence (Figures 1B–1D). This consensus helix together with α_1, α_2, and α_5 forms a hydrophobic cavity that wraps around the N terminus of eIF4E like a molecular bracelet (Figures 1C and 1D; Figures 2B and 2C). The inner diameter of the bracelet is roughly 15 Å and roomy enough to accommodate a single extended polypeptide chain (Figure 2D). Conserved residues 33–38 found in the N terminus of eIF4E (Figure 1A; Figures 2A and 2C) form a molecular "wrist" that inserts into the bracelet cavity while residues 23–32 of eIF4E become folded and emerge as turn (residues 30–32)/helix(α_1, residues 26–29)/extended chain (23–25) segment that forms a small molecular "fist" (Figures 1C and 1D; Figure 2C).

Residues from all five helices from eIF4G (393–490) contact eIF4E to make up a total of 4400 Å^2 buried surface area (Figures 2B and 2C). Importantly, eIF4G (393–490) does not contact the cap binding slot (Figure 4C). Interactions between the consensus helix, α_4, of eIF4G and helices α_3 and α_5 located on the convex dorsal surface of eIF4E are observed as in the murine eIF4E/eIF4GII-peptide complex (Marcotrigiano et al., 1999) (Figure 6A). Hydrophobic residues that line the interior of the bracelet are presented by α_1 (Ile^{416}), an adjoining loop between α_1 and α_2 (Pro^{425}, Ile^{426}), α_2 (Phe^{432}), the consensus helix α_4 (Tyr^{454}, Phe^{458}, Phe^{462}) and α_5 (Ile^{482}, Val^{483}) and contact conserved (His^{37}, Pro^{38}) or consensus hydrophobic (Val^{35} and Phe^{33}) residues in the N terminus of eIF4E (Figure 2A). These residues from yeast eIF4GI are conserved or highly similar in mammals (Figure 1B). Hydrophobic residues of the N-terminal helical turn of eIF4E (α_1: Val^{26}, Leu^{27}) form contacts with the consensus helix (Phe^{462}) and a loop between the second and third helices (Tyr^{434}) (Figure 2A) of eIF4GI. The opposite face of Phe^{462} contacts Val^{71} and Trp^{75} which is located on the convex dorsum of eIF4E, in a similar way as observed in the mammalian eIF4E/peptide complex (Marcotrigiano et al., 1999) (Figure 6A).

Hydrophobic and charged interactions are observed on the edge of the eIF4G bracelet and eIF4E. Residues from the C-terminal helix of eIF4G (Trp^{474}, Thr^{478}, Lys^{481}) interact with conserved residues in the second β strand (Phe^{68}) and third helix of eIF4E (Glu^{72}, Glu^{73}; Figures 1B and 2C). Acidic loops found N-(Asp^{125}Asp^{127}, Glu^{128}) and C-terminal (Glu^{140}, Asp^{143}, Glu^{144}) to the fifth helix of eIF4E engage basic residues found in the consensus (Lys^{463}) and third helices of eIF4G (Lys^{447}, Lys^{444}), respectively (Figure 2B). The latter region of eIF4E is conserved between mammals and yeast (Figure 1A) while Lys^{447} of eIF4G was identified previously as a functionally significant residue in a genetic screen (Hershey et al., 1999).

The N Terminus of eIF4E Is Required for Folding, Tight Binding of eIF4G (393–490), and Maintenance of a Long Lived Complex

To investigate the role of the N terminus of eIF4E for interaction with eIF4G, we have recorded a series of

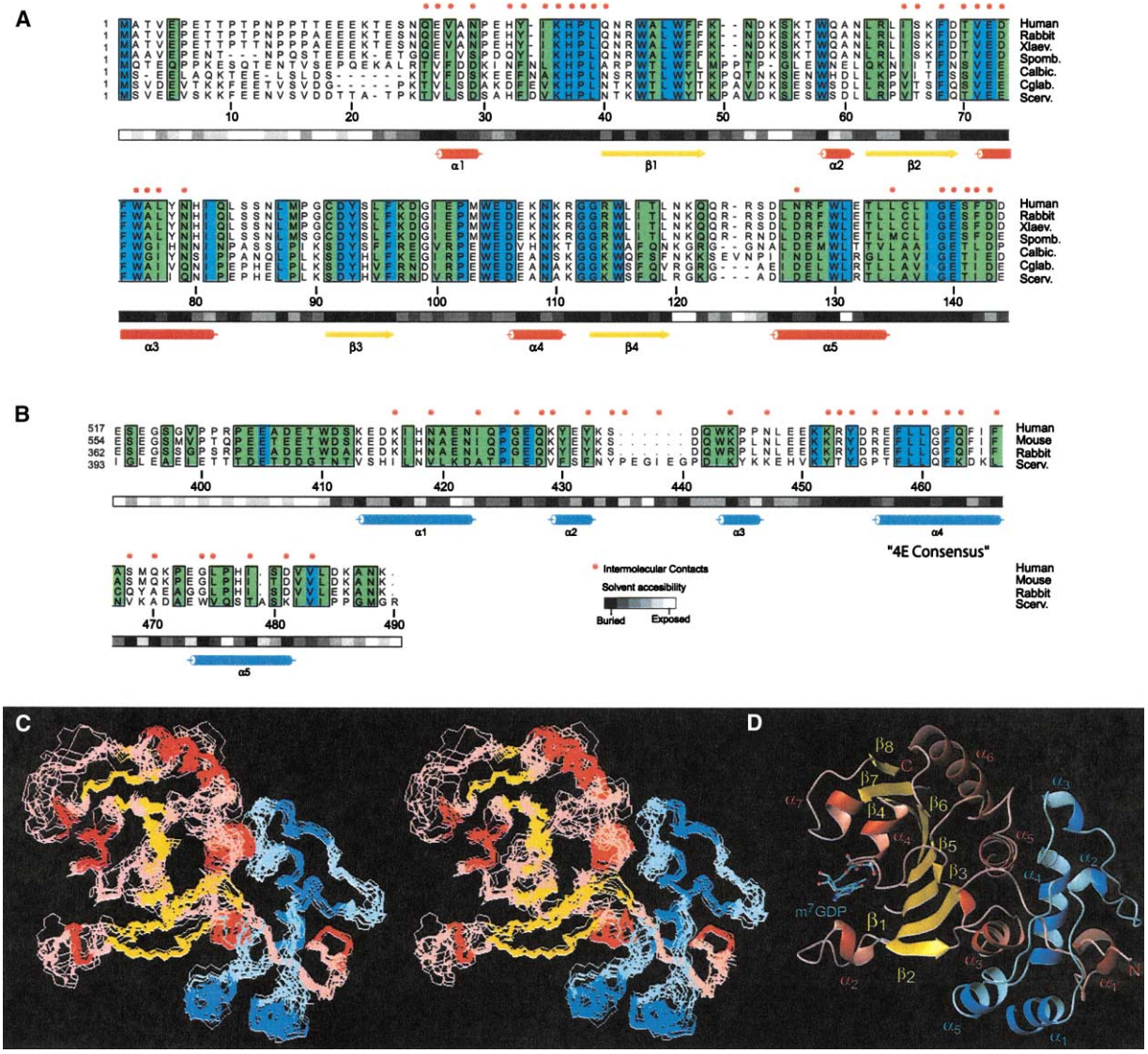

Figure 1. Interface Contacts, Stereo View, and Overall Fold of the eIF4G/eIF4G Complex

(A) Sequence alignments of eIF4E and (B) eIF4GI proteins. Only residues found in the eIF4G binding region of eIF4E are included.

(C) Superposition of 11 lowest energy structures selected out of 50 models calculated using XPLOR (Brunger, 1996) with no NOE violations greater than 0.5 Å and no angular violations greater than 5°.

(D) Ribbon diagram of eIF4E (colored red and yellow) in complex with eIF4GI (393–490) (colored blue) corresponding to lowest energy structure with lowest RMSD to the mean structure. Residues 1–23 of eIF4E and 393–413 of eIF4GI (393–490) show no long-range NOEs, appear disordered, and have been omitted for clarity. Figures prepared using Molmol (Koradi et al., 1996).

HSQC spectra of ^{15}N-labeled eIF4G (393–490) in complex with unlabeled N-terminal truncations of eIF4E (Figure 3A). eIF4G (393–490) appears mostly unfolded when mixed with either Δ35 or Δ30 eIF4E but folds as in the wild-type complex upon binding Δ20 eIF4E. This suggests that Δ20 but not Δ30 and Δ35 eIF4E would bind eIF4G (393–490). However, GST pull-down assays (Figure 3B), isothermal titration calorimetry (ITC, Figure 3C), and surface plasmon resonance (SPR, Figure 3D) indicate that eIF4G (393–490) interacts with all three deletion mutants of eIF4E but with a large variation in affinities. Wild-type and Δ20 eIF4E promote folding of eIF4G (393–490) and bind in tight complexes (k_d = 2–5 nM). In contrast, eIF4G (393–490) binds Δ30 and Δ35 eIF4E in a mostly unfolded state with significantly reduced affinity yielding dissociation constants of 66 and 250 nM, respectively. We do not understand the modest discrepancy between Δ30/eIF4G (393–490) dissociation constant measured by SPR and ITC, though data from the latter method correlate well with the stepwise exacerbation of phenotypes for the deletion mutants in vivo (see below).

In mammals, oligopeptides containing the Y(X)$_4$Lϕ consensus motif from eIF4GI and eIF4GII form tight complexes with N terminally truncated eIF4E, with measured equilibrium dissociation constants of 27 and 150 nM, respectively (Marcotrigiano et al., 1999). Strikingly, the corresponding peptide from yeast eIF4GI binds eIF4E much weaker, at 2 μM (Figure 3, left table). Nevertheless, despite weak binding of this peptide, mutations

Table 1. NMR Structural Statistics	
Restraints for Structure Calculations	
Total Restraints	3137
Total HBond Restraints	
Intramolecular 4E/4G	58/49
Intermolecular	
4E/4G	1
m^7GDP/4E	2
Total NOE Restraints	
Intramolecular 4E/4G	1698/305
Intermolecular 4E/4G	129
Intermolecular m^7GDP/4E	35
Total PB[d] Restraints (upper/lower)	
Intramolecular 4E	103/200
Intermolecular 4E/4G	32/76
Dihedral(ϕ, ψ, χ_1[c], χ_2[c]) 4E/4G	(89, 100, 60, 49)/(58, 56, 17, 20)
Statistics for Structure Calculations[b]	
Rmsd from Experimental Restraints	
Distances (Å)	0.037±.001
Angles (deg)	0.44 ± 0.05
Deviations from Idealized Geometry	
Bonds (Å)	0.002 ± 0.009
Angles (deg)	0.40 ± 0.01
Coordinate Precision (Å)	
By Subunit (eIF4E/eIF4G)	
Rmsd of backbone atoms (N, Ca, C′)	(0.82/0.68)[a] (1.40/1.25)[b]
Rmsd of heavy atoms	(1.28/0.86)[a] (1.85/1.36)[b]
Overall	
Rmsd of backbone atoms (N, Ca, C′)	0.92[a], 1.23[b]
Rmsd of heavy atoms	1.40[a], 1.79[b]
Procheck Analysis eIF4E/eIF4G (percent)	
Most favored	(73.3[a], 59.4[b])/(88.0[a], 73.9[b])
Additional allowed	(22.5, 28.3)/(9.5, 16.6)
Generously allowed	(3.8, 10.0)/(1.8, 7.5)
Disallowed region	(0.4, 2.2)/(0.7, 2.0)

[a] Regular secondary structure.
[b] Structured regions: residues 20–213 of eIF4E and/or residues 410–485 of eIF4G.
[c] Angles from secondary structure dependent χ_1, χ_2 database as Dunbrack and Karplus (1993).
[d] Paramagnetic broadening effects as in Battiste and Wagner (2000).

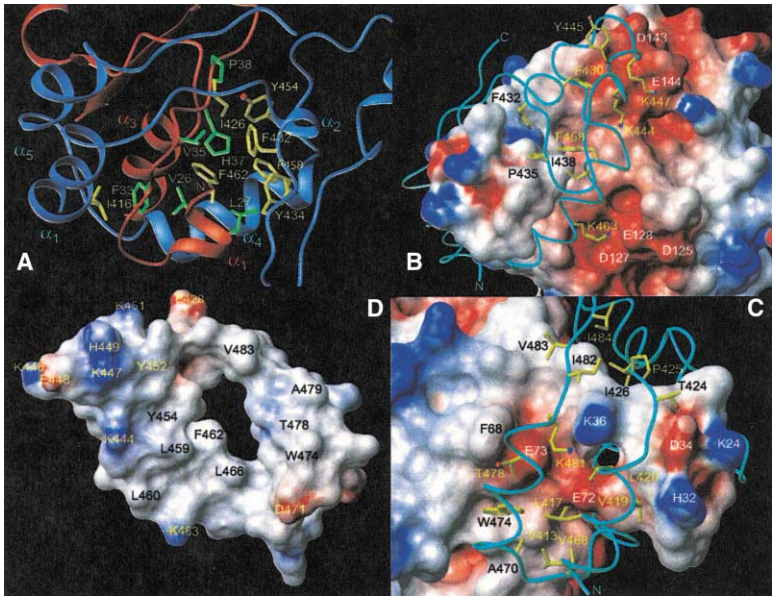

Figure 2. Intermolecular Contacts between eIF4E (red) and eIF4GI (393–490) (blue)

(A) View of dorsal surface of eIF4E showing conserved residues from the N terminus (colored in green) interacting with residues lining the hydrophobic cavity of eIF4GI (393–490) (colored yellow).

(B) eIF4G (393–490) wraps around the N terminus of eIF4E. Contact surface of eIF4E colored by electrostatic potential with eIF4G (393–490) backbone represented as a cyan ribbon showing intermolecular charged interactions and intra- and intermolecular hydrophobic interactions thought to be important for folding eIF4G (393–490).

(C) View as in (B) but rotated 90° around the vertical axis.

(D) Contact surface of eIF4G (393–490) viewed from the dorsal surface of eIF4E color coded by electrostatic potential. Note the cluster of basic residues and the large hydrophobic cavity in the center of eIF4G (393–490). Figures prepared using Molmol (Koradi et al., 1996).

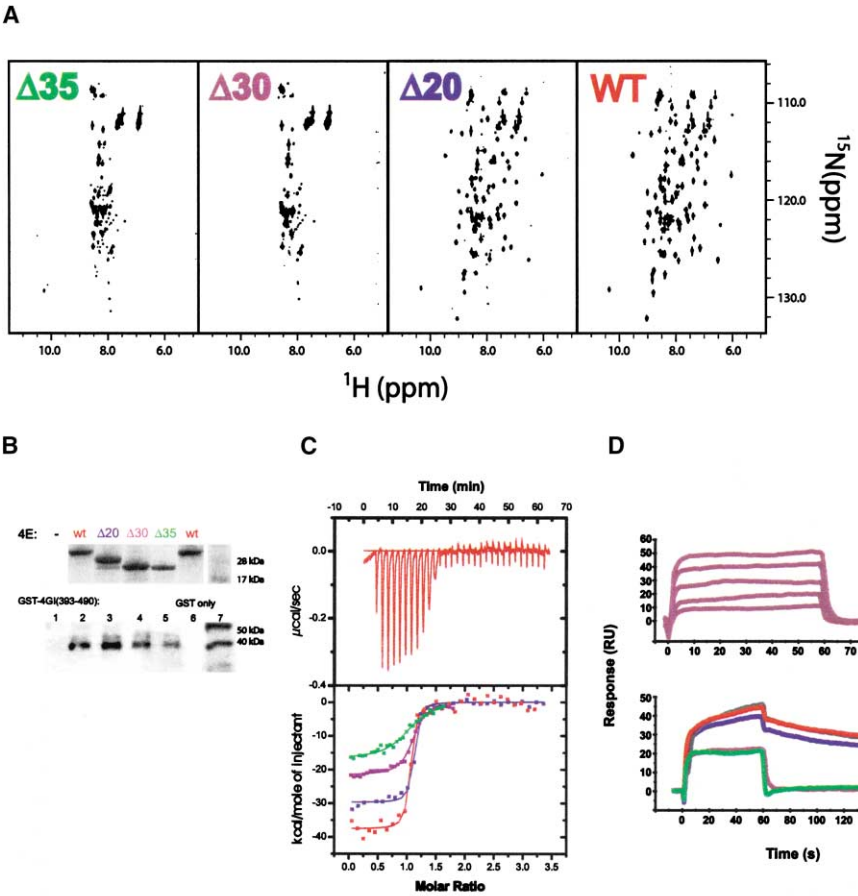

Thermodynamic parameters for eIF4E/eIF4G binding.

4E	ΔH (kcal/mol)	TΔS (kcal/mol)	ΔG (kcal/mol)	K_d (nM)
WT	-37.8	-26.3	-11.5	4.2
Δ20	-29.8	-18.4	-11.4	4.7
Δ30	-20.1	-10.3	-9.8	63.2
Δ35	-18.2	-9.1	-8.9	314.4
Δ20/(449466)	-14.5	-6.7	-7.8	2000

Kinetic parameters for eIF4E/eIF4G binding.

4E	$k_{on1}(M^{-1}\,s^{-1})$	$k_{off1}(s^{-1})$	$k_{on2}(s^{-1})$	$k_{off2}(s^{-1})$	K_d(nM)
WT	7.0×10^{6}	0.24	0.06	0.003	1.6
Δ20	1.4×10^{6}	0.15	0.05	0.002	5.4
Δ30	1.3×10^{6}	0.34	-	-	270
Δ35	3.8×10^{6}	0.97	-	-	250

Figure 3. The N Terminus of eIF4E Is Required for Folding and Tight Binding of eIF4G (393–490)

(A) ^{15}N HSQC spectra of unlabeled N-terminal deletion mutants Δ35, Δ30, Δ20 and wild-type (wt) eIF4E in complex with ^{15}N-labeled eIF4G (393–490).

(B) Western blot of GST-eIF4G (393–490) captured by m^{7}GDP immobilized wild-type and N-terminal deletants of eIF4E. Detection using anti-GST antibodies-lower image, input of eIF4E-upper image. Lanes 1 and 6 are controls corresponding to GST-4G (393–490) and GST added to unloaded and eIF4E bound m^{7}GDP, respectively.

(C) Isothermal titration calorimetry data for m^{7}GDP/eIF4E binding to eIF4G (393–490). Top: raw data for wild-type binding. Bottom: fits of integrated heat changes to one-site binding model. Binding curves corresponding to wild-type, Δ20, Δ30 and Δ35 eIF4E are colored red, blue, purple and green, respectively.

(D) Surface plasmon resonance data for wild-type and mutant m^{7}GDP/eIF4E binding to immobilized GST-eIF4G (393–490). Top: sensorgram for Δ30 mutant of eIF4E binding to GST-eIF4G (393–490) at concentrations of 50, 100, 200, 400, and 800 nM Δ30 eIF4E. Bottom: sensorgram corresponding to binding of wild-type, Δ10, Δ20, Δ30, and Δ35 eIF4E each at a concentration of 200 nM. Color-coding as in (c) but with Δ10 included and depicted in gray (nearly superimposed with wild-type data).

of signature residues of the Y(X)$_4$Lϕ motif within full-length eIF4GI abrogate binding to the phylogenetically conserved convex dorsum of eIF4E . In yeast, mutation of Tyr^{454} to Ala is lethal while replacing both Leu^{459} and Leu^{460} with Ala results in a temperature-sensitive phenotype (Tarun and Sachs, 1997). Similar mutations in mammalian eIF4GI abolish interactions with eIF4E in vitro (Mader et al., 1995). Not surprisingly, structural alignment of the consensus peptide region from yeast eIF4GI and mammalian eIF4GII in complex with yeast eIF4E gives an overall backbone RMSD of 0.6 Å indicating a conserved mode of interaction with the convex dorsum of eIF4E (Figure 6A). However, this helix constitutes only a portion of the bracelet formed by eIF4G (393–490). The interface occupied by eIF4GI (393–490) is four times larger than that occupied by the consensus peptide

providing numerous additional contacts that promote tight binding through a dramatic change in enthalpy of binding at the cost of entropy, presumably through the unfolded-to-folded transition (Figure 3, left table). Nearly half the binding enthalpy derives from the first 35 residues of eIF4E underscoring the energetic significance of this region for interaction with eIF4G (Figure 3, left table). Interestingly, that residual binding occurs in the absence of the first 35 residues of eIF4E suggests that complex formation may occur in a manner that is independent of contacts with the N-terminal appendage. The difference in binding affinity between the yeast and mammalian eIF4G consensus peptides may derive from the fact that the convex dorsum of yeast eIF4E is more charged than that of the mammalian factor.

We next wondered if formation of the bracelet architecture was slow and whether or not interaction with the N terminus of eIF4E led to a long-lived complex. Given the agreement between the dissociation constants measured by ITC and SPR, we proceeded to extract kinetic parameters from the SPR data. The interactions of wild-type, Δ10 and Δ20 eIF4E with eIF4G (393–490) are best described by a two-state binding model, while that for Δ30 and Δ35 eIF4E is best described by a simple binding model (Supplemental Figure S1 available at http://www.cell.com/cgi/content/full/115/6/739/DC1). In all cases, the initial association and dissociation rates are on the order of 10^6 s^{-1} M^{-1} and 10^{-1} s^{-1}, respectively (Figure 3, right table). For wild-type, Δ10 and Δ20, the second association and dissociation rate are on the order of 10^{-2} and 10^{-3} s^{-1} respectively. Given complete folding of eIF4G (393–490) is promoted by wild-type, Δ10, and Δ20 eIF4E, we interpret the observed two-state binding as an initial encounter followed by a collapse into a folded structure. A two-state binding model agrees well with our structural data. The inner diameter of the bracelet formed by eIF4G (393–490) is less than that of the outer diameter of the fist region of eIF4E spanned by residues 23–30 (Figure 2C). Therefore, the bracelet has to be opened (unfolded) in order to bind eIF4E followed by fastening (folding) around the N terminus of eIF4E into the complex we observe. In contrast, in the absence of N-terminal residues 1–30 of eIF4E, eIF4G (393–490) binds in a mostly unfolded state, consistent with the observed simple binding kinetics. That initial association and dissociation rates are similar for wild-type and all mutants suggests that the N terminus of eIF4E is dispensable for initial binding and that the dorsal surface of eIF4E mediates the early stages of molecular recognition. The consensus peptide, eIF4G (449–466), may participate in encounter complex formation as it binds to eIF4E with micromolar affinity (Figure 3, left table). These results document that residues 20–35 of eIF4E play a key scaffolding role by folding eIF4G (393–490). The interlocking interface thus generated promotes tight binding and slow dissociation kinetics.

Formation of the Helical Ring Spanned by eIF4G (393–490) Enhances Association of eIF4E with Capped RNA

From yeast (Ptushkina et al., 1998) to mammals (Haghighat and Sonenberg, 1997), eIF4G mediates increased association of eIF4E with capped RNA whereas the consensus peptide alone is unable to promote such an effect (Marcotrigiano et al., 1999; von der Haar et al., 2000). We next wondered if formation of the large eIF4E-eIF4G (393–490) interface affects association of eIF4E with the cap structure. A gel mobility shift assay was performed on ^{32}P-labeled capped RNA and N-terminal deletion mutants of eIF4E in the presence or absence of eIF4G (348–514) (Figures 4A and 4B). These data indicate that the association of wild-type, Δ10, and Δ20 eIF4E with capped RNA is increased in the presence of eIF4G (348–514) while that for Δ30 and Δ35 eIF4E is unaffected. Similar results were obtained with eIF4G (393–490) (Figure 4B and Supplemental Figure S2 available on *Cell* website). Since eIF4G (348–514) does not interact with RNA in this assay (von der Haar et al., 2000), we conclude that the enhanced association of eIF4E with the cap depends on N-terminal residues 20–35 of eIF4E and does not derive from interactions of eIF4G (348–514) with the RNA body.

Our NMR data confirm that the N terminus of eIF4E acts as a remote sensor for the cap binding slot. The observation that interaction of eIF4G (393–490) with eIF4E induces chemical shift changes in the cap binding site is consistent with small conformational changes in this region (Figure 4C). Thus, residues 20 to 35 of eIF4E present a scaffold for folding eIF4G allowing formation of intermolecular contacts that allosterically modulate cap binding. Regions of the eIF4E/eIF4G (393–490) interface that may be important for enhanced cap binding include residues in the wrist region (Phe^{33}, Val^{35} and His^{37}) found buried in the core of the bracelet formed by eIF4G, and residues lining the edge of eIF4E (Val^{65}, Thr^{66} and Phe^{68}) that buttress the C-terminal helix (α_5) of eIF4G (393–490) (Figures 2A and 2C; Figure 4C). Additional hydrophobic interactions between residues found in the C-terminal tail (Val^{483}) of eIF4G (393–490) and Pro^{35} of eIF4E may also be important (Figures 2A and 2C; Figure 4C). That these residues are similar or conserved in mammalian eIF4E suggests a common functional role (Figure 1A). Formation of the extensive interfacial surface area may provoke changes in slow "breathing" type motions in the vicinity of the cap binding slot, altering binding kinetics, and/or the population of cap bound. Further experiments are required to understand the details of this important mechanism.

At apparent variance with our findings are data from free eIF4E, eIF4F, and an isoform of eIF4F (iso-eIF4F) derived from wheat germ extracts that indicate a similar affinity for m^{7}GpppG (Carberry et al., 1991); however, time-resolved fluorescence studies of this interaction suggest that the dissociation rate of the m^{7}GpppG/iso-eIF4F complex is reduced relative to that with free eIF4E (Sha et al., 1995). Addition of PABP to both eIF4F and iso-eIF4F increases the affinity for the cap (Wei et al., 1998) and further reduces the off-rate for the cap interaction (Luo and Goss, 2001). The conformational coupling observed in the yeast complex may provide a mechanism for PABP to influence cap binding as observed for wheat germ eIF4F.

Studies of the mammalian factors derived from HeLa cell extracts show that eIF4E efficiently crosslinks to the cap structure and that this effect is strongly reduced upon polio virus infection (Lee and Sonenberg, 1982).

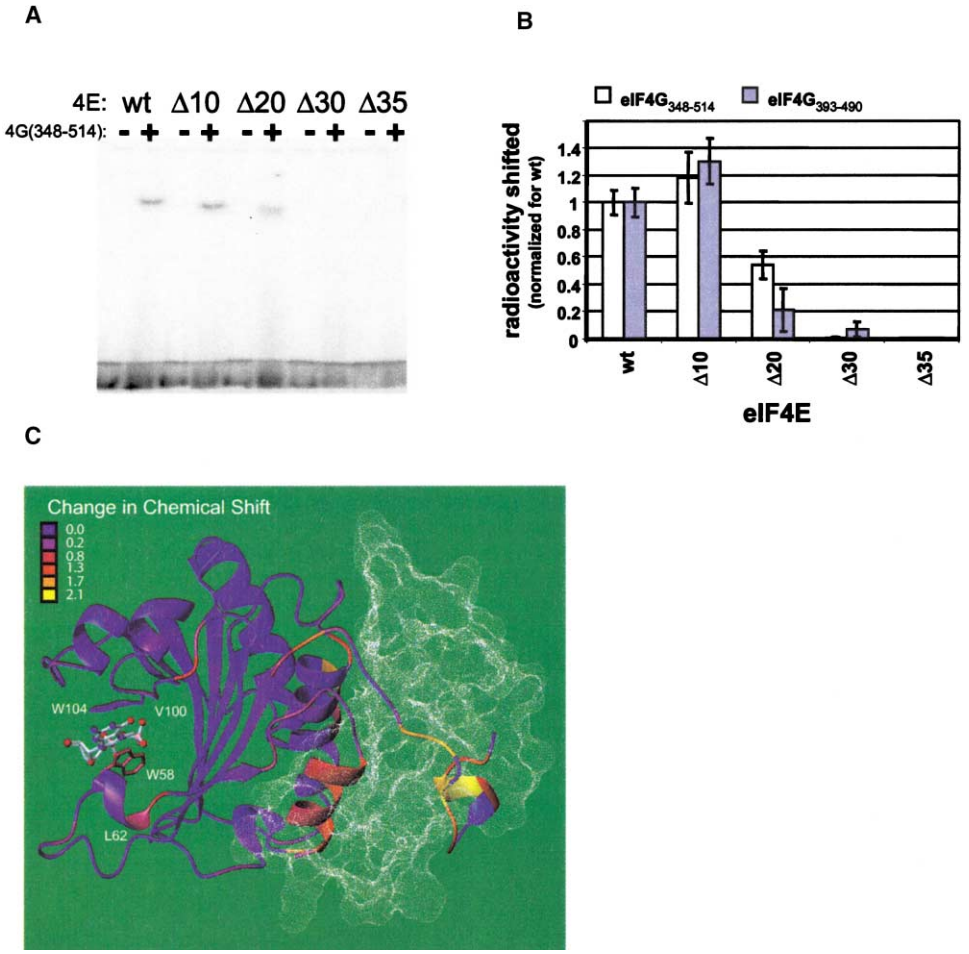

Figure 4. Folding of eIF4G (393–490) Allosterically Enhances Association of eIF4E with the Cap Structure In Vitro

(A) Gel mobility shift experiments on ^{32}P labeled capped RNA in the presence or absence of eIF4G (348–514) for indicated N-terminal deletion mutants and wild-type eIF4E.

(B) Amount of ^{32}P signal shifted relative to wild-type as in (A).

(C) Change in N, HN, and CO backbone chemical shifts between m^7GDP/eIF4E binary and m^7GDP/eIF4E/eIF4G (393–490) ternary complexes. The change in chemical is calculated as the magnitude of a vector with the components given by scaled chemical shift deviations for N, HN, and CO as using $[(\Delta N^*0.17)^2 + (\Delta C^*0.39)^2 + \Delta H^2]^{0.5}$. Side chain chemical shift changes are included for Trp^{58} and Trp^{104}. Residues of eIF4E (excluding Pro) that are unassigned in either the free-f or eIF4G bound-b form are Asp^{29}f, Ser^{30}f, Leu^{39}f, Thr^{48}b, Lys^{49}b, Arg^{97}fb, Asn^{98}b, Glu^{103}b, Gln^{148}f, Asp^{190}f, Gly^{192}b, His^{199}b, and Gln^{208}fb.

Later work formally demonstrated that recombinant eIF4G dramatically enhances association of eIF4E with capped RNA in this assay (Haghighat and Sonenberg, 1997). Since the middle domain of eIF4G supports IRES driven translation in these viruses (Pestova et al., 1996) and since the N-terminal third of eIF4G bearing the eIF4E binding domain is separated from the C-terminal two-thirds during infection (Etchison et al., 1982), it was suggested that the middle domain of eIF4G mediated increased association (Haghighat and Sonenberg, 1997). Our results indicate that enhanced association between eIF4E and eIF4G occurs at the level of cap recognition through an allosteric effect. We have shown that occupation of the dorsal surface of eIF4E is insufficient for this effect whereas proper folding of the bracelet formed by eIF4G (393–490) is required. However, we cannot exclude the possibility that association of yeast eIF4F with mRNA might be further enhanced by regions of eIF4G that contain RNA binding activity (Berset et al., 2003).

The fact that cleavage of mammalian eIF4G by picornaviral protease requires binding to eIF4E suggests that, like in yeast, complex assembly promotes a large conformational change that extends well beyond the consensus peptide (Ohlmann et al., 1997). Intriguingly, it was reported that this effect is not observed with N-terminal GST labeled eIF4E, suggesting this region plays a scaffolding role as found in the yeast factor (Ohlmann et al., 1997). Despite intimations that the N terminus of eIF4E plays a similar role in yeast and humans, it has previously been reported that the deletion of up to 33 amino acids from the N terminus of eIF4E still leaves this protein capable of supporting cap-dependent translation of reporter RNA in rabbit reticulocyte lysate immunodepleted of wild-type eIF4E (Marcotrigiano et al., 1997). The interpretation of these data, and the fact that

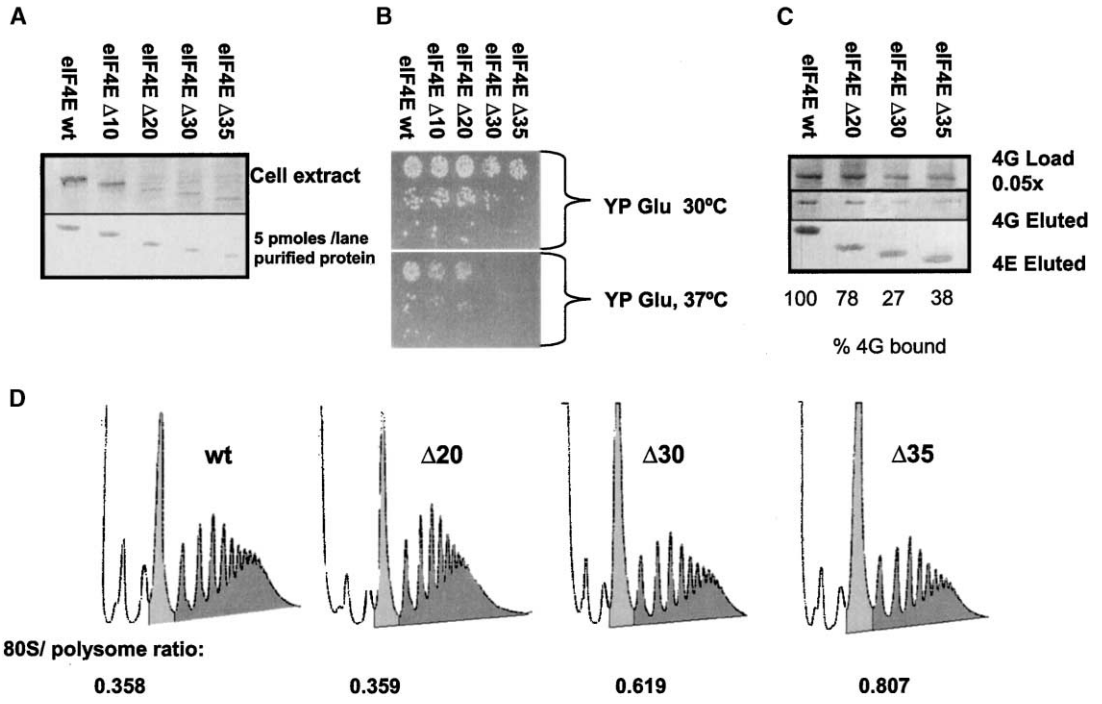

Figure 5. In Vivo Analysis of N-Terminal Deletions in eIF4E

(A) Western analysis of the intracellular eIF4E levels of the respective strains. Upper image: cell extracts with equal amounts of total protein applied, lower image: recombinant proteins with equimolar amounts applied.

(B) Growth analysis of strains containing wt or N terminally deleted copies of eIF4E. Serial dilutions (from top to bottom: 500/50/5 cells) were plated onto YP glucose plates and grown for 48 hr at the indicated temperatures.

(C) Cell extracts derived from the eIF4E deletion strains were passed over m^7GDP columns, and the bound proteins analyzed by Western blotting. Top image: cell extracts blotted for eIF4G, middle image: eluates blotted for eIF4G, lower image: eluates blotted for eIF4E. The numbers below the blots indicate the amount of eluted eIF4G normalized to wild-type, and corrected for variations in the amount of loaded eIF4G, as quantified by analysis of the band densities.

binding of the consensus peptide to eIF4E is tight, was that the first 33 residues of mammalian eIF4E were dispensable for function and that recognition between the two factors was mediated by the consensus peptide and contacts with the convex dorsum of eIF4E. However, it is not clear what the levels of mutant eIF4E were in this study; if amounts were abnormally high, any defect in cap-dependent translation would have been compensated by a mechanism not unlike the dose compensation observed in vivo for the truncation mutants of yeast eIF4E (Vasilescu et al., 1996). Perhaps more importantly, the remaining residues of mammalian eIF4E (Tyr^{34}, Ile^{35} and His^{37} and Pro^{38}) correspond to those of yeast eIF4E found buried in the core of the cavity formed by eIF4G (393–490) (Figures 1A, 2A, and 4C). It is possible that residues of the wrist region spanning from 33–39 form a conserved core interface in all eukaryotes while those in the helical fist region spanned by residues 23–30 form a variable interface, whose function may be species specific. Further experiments will be required in order to investigate the importance of these regions for mammalian translation initiation.

The N Terminus of eIF4E Is Required for Optimal Growth and Maintenance of Polysomal Structure

In order to address the function of the interlocking bracelet architecture observed in our structure, we constructed yeast strains containing as only source of eIF4E wild-type or N terminally deleted versions of this protein expressed from a TRP1 promoter, which has expression levels comparable to the endogenous *CDC33*-promoter (Vasilescu et al. 1996). While strains containing Δ10 and Δ20 eIF4E were indistinguishable from the wild-type strain when grown in rich medium, Δ30 and Δ35 strains showed a reduction in growth rates (Supplemental Figures S3A and S3B available on *Cell* website). Western analysis performed on these yeast strains showed that expression levels of the various forms of eIF4E were comparable (Figure 5A). Note that the apparently lower band intensities obtained with the deletion mutants stem from variations in antibody reactivity, since a comparable loss in intensity is observed with a standard where equal molar amounts of the eIF4E mutants were applied to the gel. These data are consistent with the observation that the first twenty amino acids of eIF4E contain a prominent antigenic motif (Ptushkina et al. 1998). Phenotypic differences between the strains are therefore related to functional differences in the various deletion mutants, rather than different expression levels.

The observed reduction in growth rate for Δ30 and Δ35 eIF4E was greatly exacerbated at elevated temperatures (Figure 5B), as well as in other suboptimal growth conditions such as with galactose as only carbon source or under osmotic stress (data not shown). Consistent with the notion that these phenotypes are produced by an

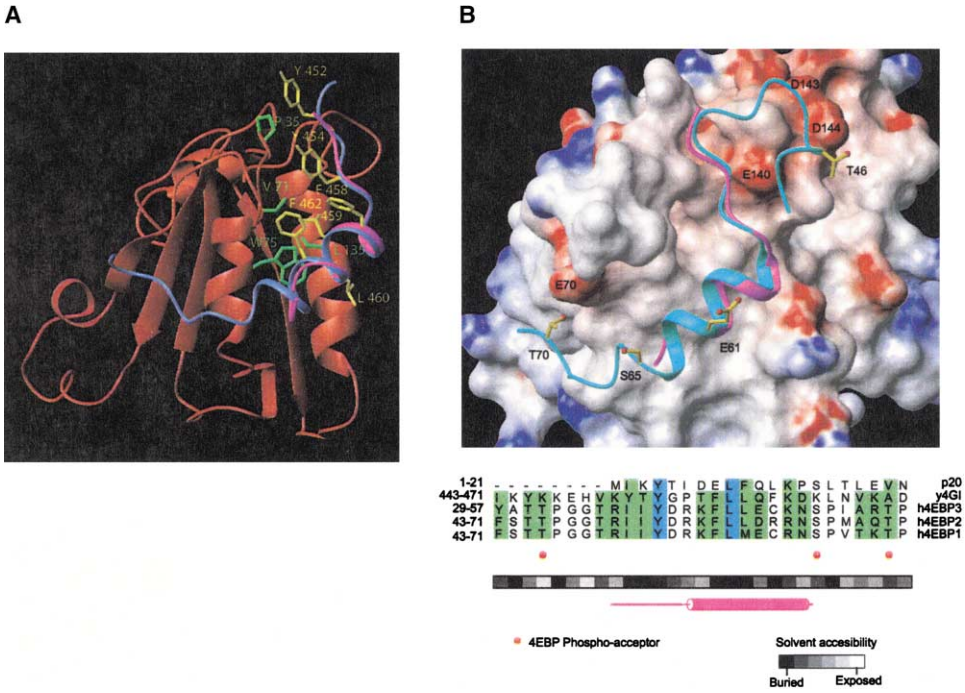

Figure 6. Model of 4E-BP Regulation of Translation Based on the Yeast eIF4G/eIF4G (393–490) Complex

(A) Overlay of yeast eIF4E (red)/eIF4GI (blue) residues 451 to 472 with mammalian eIF4GII (magenta) residues 621 to 634 (PDB code 1EJH). Alignment based on yeast eIF4GI residues 454 to 462 containing the Y(X)$_4$Lϕ motif. Note ϕ = L in the mammalian and yeast eIF4GI consensus motif. Conserved residues of eIF4E depicted in green; eIF4G residues depicted in yellow. Backbone rmsd over aligned region 0.6 Å.

(B) Homology model of human eIF4E in complex with human 4E-BP1. Displayed is a contact surface between modeled human eIF4E colored by electrostatic potential. Mammalian 4E-BP1, from the cocrystal structure with murine eIF4E (magenta) is superimposed with a model of human 4E-BP1 (cyan) with a backbone RMSD of 1 Å. In yellow are three phosphoacceptor sites-Thr^{70}, Ser^{65}, and Thr^{46}-along with Glu^{61}. Thr^{46} of 4E-BP1 interacts with Asp^{144} of eIF4E. Residues Ser^{65} and Thr^{70} of 4E-BP1 are oriented toward Glu^{70} of heIF4E. Ser^{65} is also in close proximity to Glu^{61} and may destabilize formation of the consensus helix in addition to providing electrostatic repulsion from Glu^{70} from eIF4E.

impairment in the eIF4E:eIF4G interaction, eluates from m^{7}GDP columns showed reduced levels of eIF4G copurified from the slower-growing strains, despite the fact that the cellular eIF4G content was not significantly altered (Figure 5C). These data indicate a reduced stability of eIF4E:eIF4G complexes in the Δ30 and Δ35 strains. Analysis of polysomal profiles confirms that the same mutants show increased 80S:polysome ratios, as is to be expected from a defect in the translation initiation machinery (Figure 5D). Our results demonstrate that regions of eIF4E required for complete folding of eIF4G (393–490) and allosteric enhancement with capped RNA in vitro also play a key role in supporting growth and maintenance of polysomal structure in vivo.

Regulation of Translation by the 4E-BPs

We next wondered if conserved surface residues of eIF4E that contact eIF4G (393–490) are employed during regulation of the eIF4E/4E-BP interaction. Crystallographic analysis on 16 residue peptides from either mammalian eIF4GII or 4E-BP1 in complex with N terminally truncated murine eIF4E show that the 4E-BPs mimic at least a portion of the eIF4G binding site (Marcotrigiano et al., 1999). However, absent from these data are the positions of the phosphoacceptor sites of 4E-BP relative to eIF4E. The 4E-BP1 peptide binding surface on eIF4E (Marcotrigiano et al., 1999) is overlapping with, but smaller than, that previously determined by NMR chemical shift mapping with full-length 4E-BP1 (Matsuo et al., 1997). This NMR derived binding site of 4E-BP1 overlaps with the binding site of eIF4GI (393–490) for yeast eIF4E in two regions containing conserved acidic residues: Glu^{72}, Glu^{73}, and Glu^{140}/Asp^{143}/Glu^{144} (Figure 1A). Given these data, we were prompted to construct a homology model of human 4E-BP1/eIF4E comprising eight and six residues N- and C-terminal to the consensus peptide, respectively (Figure 6B). This is of interest since hyperphosphorylation of 4E-BP1 that regulates association with eIF4G is likely to occur while in complex with eIF4E (Gingras et al., 1999a).

The major phosphorylation sites on 4E-BP1 identified in human embryonic kidney 293 cells are Thr^{36}, Thr^{46}, Ser^{65}, and Thr^{70} (Gingras et al., 2001). The latter three sites appear in our model and point toward the aforementioned conserved acidic patches of eIF4E (Figure 6B). A variety of biophysical methods indicate that 4E-BP1 monophosphorylated on Ser^{65} (Gingras et al., 2001; Karim et al., 2001; Niedzwiecka et al., 2002) or diphosphorylated Ser^{65} and Thr^{70} (Gingras et al., 2001; Niedzwiecka et al., 2002) have submicromolar dissociation constants with eIF4E. Additional phosphoacceptor sites on 4E-BP, such as Thr^{46}, would be required for complete liberation of eIF4E. Phosphorylation of 4E-BP1 is ordered and hierarchical: Thr^{36} and Thr^{46} are phosphorylated prior to Thr^{70}, which is followed by phosphorylation of Ser^{65} (Gingras et al., 2001). Our model shows that

Thr[46] is more exposed than Ser[65] and Thr[70] (Figure 6B). If 4E-BP1 is phosphorylated while in complex with eIF4E, it is possible that the order of phosphorylation is based on accessibility. Upon phosphorylation of the N-terminal sites, the off-rate of 4E-BP is increased, allowing access to C-terminal phosphoacceptor sites.

Regions outside of the 4E-BP consensus sequence may also effect association of eIF4E with the cap structure. SPR studies show that both 4E-BP1 (Scheper et al., 2002) and 4E-BP2 (Ptushkina et al., 1999) are capable of dramatically reducing the off-rate of eIF4E from a cap-RNA coated sensor chip. In contrast, 4E-BP1 is unable to induce crosslinking of eIF4E to capped RNA unlike the strong effect induced by eIF4G (Haghighat and Sonenberg, 1997). The discrepancies between the crosslinking and SPR results may reflect different sensitivities of the techniques. The available data suggest that the 4E-BP mediated effects are weaker than that of eIF4G. Though HSQC analysis indicates 4E-BP is mostly unstructured upon binding eIF4E (Fletcher et al., 1998), these data do not rule out regions of local secondary structure or transient contacts that may play an important role in translational regulation. Additional NMR structural and mobility studies of 4E-BP in complex with eIF4E will be necessary to address these effects.

Conclusion

We have shown that yeast eIF4G (393–490) wraps around the N terminus of eIF4E upon binding, forming a molecular bracelet. N-terminal residues 24–35 of eIF4E become structured upon binding eIF4G and are required for the folding of eIF4G (393–490). A virtue of the unusual bracelet architecture is in production of a large interface enabling slow dissociation kinetics and allosteric modulation of cap binding. Residues of eIF4E that promote folding of eIF4G (393–490) and enhanced association with the cap structure are required for optimal growth and maintenance of polysome structure in vivo. Functionally significant basic residues found on the periphery of the bracelet interact with conserved acidic regions found on the dorsal surface of eIF4E and may play a role in regulation of translation by the 4E-BPs. A model of a 4E-BP1 fragment based on the yeast eIF4E/eIF4GI (393–490) structure predicts that three of the four physiologically relevant phosphoacceptor sites are proximal to conserved acidic regions of eIF4E and that these sites are phosphorylated in order of solvent accessibility.

Our results imply that eIF4G functions not merely as a passive scaffold that coordinates proteins that bind and process mRNA during translation initiation. Rather, the conformational coupling and resulting interface between eIF4E and eIF4G observed here very likely promotes a stable mRNP which may function, in part, by promoting multiple rounds of ribosomal loading. The structure of the eIF4E/eIF4G (393–490) complex shows that assembly of eIF4F must entail a large conformational change: the inner diameter of the bracelet formed by eIF4G (393–490) is less than the outer diameter of the fist formed by eIF4E. Given the effects of Pab1p on translation and RNA decay, it is tempting to speculate that the complex we observe is further stabilized by the Pab1p/eIF4G interaction through conformational changes within eIF4G. This would allow access to the cap to be controlled and also provide a mechanism for activities at the 3′ end to influence the stability of the mRNP formed by eIF4F and Pab1p. Exploration of the structural basis for these effects is a challenge for the future.

Experimental Procedures

Structure Determination

A total of 50 structures of eIF4G (393–490) were calculated based on 367 intramolecular NOE derived distance restraints, 36 hydrogen bonds, and 84 TALOS (Cornilescu et al., 1999) derived ϕ/ψ restraints using the program XPLOR (Brunger, 1996). Side chain $\chi 1$ and $\chi 2$ restraints based on previously derived secondary structure dependent values (Dunbrack, 1993). Structures of eIF4E were calculated using a modified NOE data set consisting of NOE-derived intermolecular and intramolecular distance restraints obtained for residues 40–213 of free eIF4E:m7GDP complex as described (Matsuo et al., 1997). Side chain-to-backbone NOEs for residues in the 4G binding site (identified by chemical shift mapping) within this region were removed. Chemical shift mapping, H^N-H^N NOE analysis, and secondary chemical shift analysis at the level of chemical shift index indicate minimal changes in backbone secondary structure and β-strand pairing for residues 40–213 of eIF4E. De novo NOE and TALOS (Cornilescu et al., 1999) ϕ/ψ data were included for N-terminal residues 24–39. The lowest energy structure without any NOE or angle violations greater 0.5 Å and 5° was used for complex calculations with eIF4G (393–490). The full complex was calculated using a single m^7GDP/eIF4E structure from above with all 50 eIF4G (393–490) structures, which were added at random distances and orientations relative to m^7GDP/eIF4E. The structure quality was assessed with PROCHECK-NMR (Laskowski et al., 1993). Details regarding sample preparation, NMR spectroscopy and 4E-BP homology modeling can be found in the Supplemental Data available on *Cell* website.

Mutagenesis, RNA Gel Mobility Shift, and Protein Interaction Assays

Deletion mutants of eIF4E were prepared by PCR and verified using forward and reverse dideoxy sequencing. RNA gel shift assays were performed as described (von der Haar et al., 2000) but with a 1 mM EDTA, 45 mM Tris-borate, and pH 8 buffer. Information regarding ITC, SPR, and GST-pull-down assays can be found in the Supplemental Data available on *Cell* website.

Yeast Strains and In Vivo Analyses

A haploid yeast strain (MATa *leu cdc33:LEU trp ura* [pURA CDC33]) (Altmann et al., 1987) was transformed with centromeric plasmids containing a TRP-marker and wt or mutant eIF4E under control of the TRP1-promoter (Oliveira et al., 1993). The transformants were grown in liquid SC–Trp medium for 12 hr and then plated onto SC–Trp plates supplemented with 5-FOA (Boeke et al., 1987). Colonies growing on this medium were used for further analysis. Western blots, isolation of cap binding complexes, and polysomal gradients were performed as described (von der Haar and McCarthy, 2002).

Acknowledgments

We thank Drs. H. Matsuo, J. Battiste, J. Sun, C. Freund, and S. Buratowski for helpful discussions throughout the course of this work; the Harvard-MIT Center for Magnetic Resonance; and financial support from the National Institutes of Health (grants CA68262, CA68262, GM47467, and RR00995) and Human Frontiers in Science program. J.D.G acknowledges support from an American Cancer Society postdoctoral fellowship. J.E.G.M. and T.v.d.H. thank the Wellcome Trust (UK) and the BBSRC (UK) for support.

Received: June 27, 2003
Revised: November 10, 2003
Accepted: November 14, 2003
Published: December 11, 2003

References

Altmann, M., Handschin, C., and Trachsel, H. (1987). mRNA cap-binding protein: cloning of the gene encoding protein synthesis initiation factor eIF-4E from *Saccharomyces cerevisiae*. Mol. Cell. Biol. *7*, 998–1003.

Altmann, M., Schmitz, N., Berset, C., and Trachsel, H. (1997). A novel inhibitor of cap-dependent translation initiation in yeast-p20 competes with eIF4E for binding to eIF4E. EMBO J. *16*, 1114–1121.

Asano, K., Shalev, A., Phan, L., Nielsen, K., Clayton, J., Valasek, L., Donahue, T.F., and Hinnebusch, A.G. (2001). Multiple roles for the C-terminal domain of eIF5 in translation initiation complex assembly and GTPase activation. EMBO J. *20*, 2326–2337.

Battiste, J.L., and Wagner, G. (2000). Utilization of site-directed spin labeling and high-resolution heteronuclearnuclear magnetic resonance for global fold determination of large proteins with limited nuclear overhauser effect data. Biochemistry *39*, 5355–5365.

Benne, R., and Hershey, J.W.B. (1976). Purification and characterization of initiation factor IF-E3 from rabbit reticulocytes. Proc. Natl. Acad. Sci. USA *73*, 3005–3009.

Berset, C., Zurbriggen, A., Djafarzadeh, S., Altmann, M., and Trachsel, H. (2003). RNA-binding activity of translation initiation factor eIF4G1 from Saccharomyces cerevisiae. RNA *9*, 871–880.

Boeke, J.D., Trueheart, J., Natsoulis, G., and Fink, G.R. (1987). 5-fluoroorotic acid as a selective agent in yeast molecular genetics. Methods Enzymol. *154*, 164–165.

Brunger, A.T. (1996). X-PLOR Version 3.851: a system for X-ray crystallography and NMR (New Haven, CT: Yale University Press).

Carberry, S.E., Darzynkiewicz, E., and Goss, D.J. (1991). A comparison of the binding of methylated cap analogues to wheat germ protein synthesis initiation factors 4F and (Iso)4F. Biochemistry *30*, 1624–1627.

Cornilescu, G., Delaglio, F., and Bax, A. (1999). Protein backbone angle restraints from searching a database for chemical shift and sequence homology. J. Biomol. NMR *13*, 289–302.

Dever, T.E. (2002). Gene-specific regulation by general translation factors. Cell *108*, 545–556.

Dunbrack, R.L., and Karplus, M. (1993). Backbone-dependent rotamer library for proteins. Application to side-chain prediction. J. Mol. Biol. *230*, 543–574.

Etchison, D., Milburn, S.C., Edery, I., and Sonenberg, N. (1982). Inhibition of HeLa cell protein synthesis following poliovirus infection correlates with the proteolysis of a 220,000 Da polypeptide associated with eukaryotic initiation factor 3 and a cap binding complex. J. Biol. Chem. *257*, 14806–14810.

Fletcher, C.M., McGuire, A.M., Gingras, A.-C., Li, H., Matsuo, H., Sonenberg, N., and Wagner, G. (1998). 4E binding proteins inhibit the translation factor eIF4E without folded structure. Biochemistry *37*, 9–15.

Gallie, D.R. (1991). The cap and poly(A) tail function synergistically to regulate mRNA translational efficiency. Genes Dev. *5*, 2108–2116.

Gingras, A.-C., Gygi, S.P., Raught, B., Polakiewicz, R.D., Abraham, R.T., Hoekstra, M.F., Aebersold, R., and Sonenberg, N. (1999a). Regulation of 4E–BP1 phosphorylation: a novel two-step mechanism. Genes Dev. *13*, 1422–1437.

Gingras, A.-C., Raught, B., and Sonenberg, N. (1999b). eIF4 initiation factors: effectors of mRNA recruitment to ribosomes and regulators of translation. Annu. Rev. Biochem. *68*, 913–963.

Gingras, A.-C., Raught, B., Gygi, S.P., Niedzwiecka, A., Miron, M., Burley, S.K., Polakiewicz, R.D., Wyslouch-Cieszynska, A., Aebersold, R., and Sonenberg, N. (2001). Hierarchical phosphorylation of the translation inihibitor 4E–BP1. Genes Dev. *15*, 2852–2864.

He, H., von der Haar, T., Singh, C.R., Ii, M., Li, B., Hinnebusch, A.G., McCarthy, J.E., and Asano, K. (2003). The yeast eukaryotic initiation factor 4G (eIF4G) HEAT domain interacts with eIF1 and eIF5 and is involved in stringent AUG selection. Mol. Cell. Biol. *23*, 5431–5445.

Haghighat, A., and Sonenberg, N. (1997). eIF4G dramatically enhances the binding of eIF4E to the mRNA 5′-cap structure. J. Biol. Chem. *272*, 21677–21680.

Haghighat, A., Mader, S., Pause, A., and Sonenberg, N. (1995). Repression of cap-dependent translation by 4E-binding protein 1: competition with p220 fo rbinding to eukaryotic initation factor-4E. EMBO J. *14*, 5701–5709.

Hentze, M.W. (1997). eIF4G: a multipurpose ribosome adapter. Science *275*, 500–501.

Hershey, J.W.B., and Merrick, W.C. (2000). The pathway and mechanism of initiation of protein synthesis. In Translational Control of Gene Expression, N. Sonenberg, J.W.B. Hershey, and M.B. Mathews, eds. (Cold Spring Harbor, NY: Cold Spring Harbor Laboratory Press).

Hershey, P.E.C., McWhirter, S.M., Gross, J.D., Wagner, G., Alber, T., and Sachs, A.B. (1999). The cap-binding protein eIF4E promotes folding of a functional domain of yeast translation initiation factor eIF4G1. J. Biol. Chem. *274*, 21297–21304.

Iizuka, N., Najita, L., Franzusoff, A., and Sarnow, P. (1994). Cap-dependent and cap-independent translation by internal initiation of mRNAs in cell extracts prepared from Saccharomyces cerevisiae. Mol. Cell. Biol. *14*, 7322–7330.

Jacobson, A. (1996). Poly(A) metabolism and translation: the closed loop model. In Translational Control, J.W.B. Hershey, M.B. Matthews, and N. Sonenberg, eds. (Cold Spring Harbor, NY: Cold Spring Harbor Laboratory Press).

Karim, M.M., Hughes, J.M.X., Warwicker, J., Scheper, G.C., Proud, C.G., and McCarthy, J.E.G. (2001). A quantitative molecular model for modulation of mammalian translation by the eIF4E-binding protein 1. J. Biol. Chem. *276*, 20750–20757.

Koradi, R., Billeter, M., and Wüthrich, K. (1996). MOLMOL: a program for display and analysis of macromolecular structures. J. Mol. Graph. *14*, 51–55.

Lamphear, B.J., Kirchweger, R., Skern, T., and Rhoads, R.E. (1995). Mapping of functional domains in eukaryotic protein synthesis initiation factor 4G (eIF4G) with picornaviral proteases. J. Biol. Chem. *270*, 21975–21983.

Laskowski, R.A., MacArthur, R.W., Moss, D.S., and Thorton, J.M. (1993). PROCHECK: a program to check the sterochemical quality of protein structures. J. Appl. Crystallogr. *26*, 283–291.

Lee, K.A.W., and Sonenberg, N. (1982). Inactivation of cap-binding proteins accompanies the shut-off of host protein synthesis by poliovirus. Proc. Natl. Acad. Sci. USA *79*, 3447–3451.

Luo, Y., and Goss, D.J. (2001). Homeostasis in mRNA initiation. J. Biol. Chem. *276*, 43083–43086.

Mader, S., Lee, H., Pause, A., and Sonenberg, N. (1995). The translation initiation factor eIF4E binds to a common motif shared by the translation factor eIF4E and the translational repressors 4E-binding proteins. Mol. Cell. Biol. *15*, 4990–4997.

Marcotrigiano, J., Gingras, A.-C., Sonenberg, N., and Burley, S.K. (1997). Cocrystal structure of the messenger RNA 5′ cap-binding protein (eIF4E) bound to 7-methyl-GDP. Cell *89*, 951–961.

Marcotrigiano, J., Gingras, A.-C., Sonenberg, N., and Burley, S.K. (1999). Cap-dependent translation initiation in eukaryotes is regulated by a molecular mimic of eIF4G. Mol. Cell *3*, 707–716.

Matsuo, H., Li, H., McGuire, A.M., Fletcher, C.M., Gingras, A.-C., Sonenberg, N., and Wagner, G. (1997). Structure of translation factor eIF4E bound to m7GDP and interaction with 4E-binding protein. Nat Struct Biol *4*, 717-724.

Niedzwiecka, A., Marcotrigiano, J., Stepinski, J., Jankowska-Anyszka, M., Wyslouch-Cieszynska, A., Dadlez, M., Gingras, A.-C., Mak, P., Darzynkiewicz, E., Sonenberg, N., et al. (2002). Biophysical studies of eIF4E cap-binding protein: recognition of mRNA 5′ cap structure and synthetic fragments of eIF4G and 4E–BP1 proteins. J. Mol. Biol. *319*, 615–635.

Ohlmann, T., Pain, V.M., Wood, W., Rau, M., and Morley, S.J. (1997). The proteolytic cleavage of eukaryotic initiation factor (eIF) 4G is prevented by eIF4E binding protein (PHAS-I;4E–BP1) in reticulocyte lysate. EMBO J. *16*, 844–855.

Oliveira, C.C., van den Heuvel, J.J., and McCarthy, J.E. (1993). Inhibition of translational initiation in Saccharomyces cerevisiae by sec-

ondary structure: the roles of the stability and position of stem-loops in the mRNA leader. Mol. Microbiol. *9*, 521–532.

Pause, A., Belsham, G.J., Gingras, A.C., Donze, O., Lin, T.A., Lawrence, J.C., Jr., and Sonenberg, N. (1994). Insulin-dependent stimulation of protein synthesis by phosphorylation of a regulator of 5′ cap function. Nature *371*, 762–767.

Pestova, T.V., Shatsky, I.N., and Hellen, C.U. (1996). Functional dissection of eukaryotic initiation factor 4F: the 4A subunit and the central domain of the 4G subunit are sufficient to mediate internal entry of 43S preinitiation complexes. Mol. Cell. Biol. *16*, 6870–6878.

Prevot, D., Darlix, J.-L., and Ohlmann, T. (2003). Conducting the initiation of protein synthesis: the role of eIF4G. Biol. Cell. *95*, 141–156.

Ptushkina, M., von der Haar, T., Vasilescu, S., Frank, R., Birkenhager, R., and McCarthy, J.E. (1998). Cooperative modulation by eIF4G of eIF4E-binding to the mRNA 5′ cap in yeast involves a site partially shared by p20. EMBO J. *17*, 4798–4808.

Ptushkina, M., von der Haar, T., Karim, M.M., Hughes, J.M., and McCarthy, J.E. (1999). Repressor binding to a dorsal regulatory site traps human eIF4E in a high cap-affinity state. EMBO J. *18*, 4068–4075.

Raught, B., Gingras, A.-C., and Sonenberg, N. (2000). Regulation of ribosomal recruitment in eukaryotes. In Translational Control of Gene Expression, N. Sonenberg, J.W.B. Hershey, and M.B. Mathews, eds. (Cold Spring Harbor, NY: Cold Spring Harbor Laboratory Press).

Richter, J.D. (2000). Influence of polyadenylation-induced translation on metazoan development and neuronal synaptic function. In Translational Control of Gene Expression, N. Sonenberg, J.W.B. Hershey, and M.B. Mathews, eds. (Cold Spring Harbor, NY: Cold Spring Harbor Press), pp. 785.

Sachs, A.B., Sarnow, P., and Hentze, M.W. (1997). Starting at the beginning, middle and end, translation initiation in eucaryotes. Cell *89*, 831–838.

Scheper, G.C., van Kollenburg, B., Hu, J., Luo, J., Goss, D.J., and Proud, C.G. (2002). Phosphorylation of eukaryotic initiation factor 4E markedly reduces its affinity for capped mRNA. J. Biol. Chem. *277*, 3303–3309.

Sha, M., Wang, Y., Xiang, T., van Heerden, A., Browning, K.S., and Goss, D.J. (1995). Interaction of wheat germ protein synthesis initiation factor eIF-(iso)4F and its subunits p28 and p86 with m7GTP and mRNA analogues. J. Biol. Chem. *270*, 29904–29909.

Tarun, S.Z., and Sachs, A.B. (1997). Binding of eukaryotic translation initiation factor 4E (eIF4E) to eIF4G represses translation of uncapped mRNA. Mol. Cell. Biol. *17*, 6876–6886.

Uchida, N., Hoshino, S.-I., Imataka, H., Sonenberg, N., and Katada, T. (2002). A novel role fo the mammalian GSPT/eRF3 associating with poly(A)-binding protein in cap/poly(A)-dependent translation. J. Biol. Chem. *277*, 50286–50292.

Vasilescu, S., Ptushkina, M., Linz, B., Muller, P.P., and McCarthy, J.E.G. (1996). Mutants of eukaryotic initiation factor eIF4E with altered mRNA cap binding specificity reprogram mRNA selection by ribosomes in Saccharomyces cerevisiae. J. Biol. Chem. *271*, 7030–7037.

von der Haar, T., and McCarthy, J.E.G. (2002). Intracellular translation initiation factor levels in Saccharomyces cerevisiae and their role in cap-complex function. Mol. Microbiol. *2*, 531–544.

von der Haar, T., Ball, P.D., and McCarthy, J.E.G. (2000). Stabilization of eukaryotic initiation factor 4E binding to the mRNA 5′-cap by domains of eIF4G. J. Biol. Chem. *275*, 30551–30555.

Wei, C.-C., Balasta, M.L., Ren, J., and Goss, D.J. (1998). Wheat germ poly(A) binding protein enhances the binding affinity of eukaryotic initiation factor 4F and (iso)4F for cap analogues. Biochemistry *37*, 1910–1916.

Wells, S.E., Hillner, P.E., Vale, R.D., and Sachs, A.B. (1998). Circularization of mRNA by eukaryotic translation initiation factors. Mol. Cell *2*, 135–140.

Accession Numbers

Coordinates have been deposited in the protein data bank under the accession code 1RF8.